

# Effects of Finite Volume Reconstruction Scheme on 1D Viscous Burgers Turbulence

Josh R. Braun\*

Oklahoma State University, Stillwater, OK, 74078

This paper presents several solution schemes to the 1D Burgers turbulence problem. The primary method for comparing the schemes is to analyze the kinetic energy spectrum after a certain period of time to observe how much energy dissipation each scheme has on the solution. Generally, less dissipation is considered better, however it is also taken into consideration that some numerical schemes introduce dispersion error, which is considered worse. Of the various finite volume reconstruction schemes that were studied, the MUSCL-KT scheme without a limiter was shown to have the least dissipation and dispersion for a given spatial resolution.

## I. Nomenclature

$\alpha_k$	= non-linear weight for WENO schemes
$\beta_k$	= smoothness indicator for WENO schemes
$c_{i+1/2}$	= wave speed at the cell interface
$d_k$	= linear weight for WENO schemes
$E(k)$	= energy spectrum in wavenumber space
$E(t)$	= total kinetic energy at time $t$
$F_{i+1/2}$	= flux at the cell interface
$i$	= cell-centered node index in physical space
$k$	= cell-entered node index in wavenumber space
$n$	= time index
$\phi$	= limiter function
$q_i$	= cell-centered quantity
$q_{i+1/2}^R$	= quantity at cell interface using nodes primarily to the right of $i$
$q_{i+1/2}^L$	= quantity at cell interface using nodes primarily to the left of $i$
$u$	= velocity
$w_k$	= non-linear weight for WENO schemes

## II. Introduction

THE 1D Burgers turbulence problem is governed by a simplified form of the incompressible Navier-Stokes equation, making the rapid exploration of various numerical schemes possible. It provides a simple, benchmark problem to begin the study of turbulence and the methods for finding solutions. This study will focus on finite volume reconstruction-based solvers and comparing their effects on the kinetic energy of the problem domain.

## III. Problem Description

### A. Governing Equation

The governing equation for Burgers turbulence is essentially a simplified, 1D form of the incompressible Navier-Stokes equation:

$$\frac{\partial u}{\partial t} + u \frac{\partial u}{\partial x} = \nu \frac{\partial^2 u}{\partial x^2} \quad (1)$$

---

\*MS Student, OSU MAE Department, josh.braun@okstate.edu

This formulation makes analysis of different solution schemes simpler than the corresponding 3D, compressible Navier-Stokes equation. Because this equation is flux-conservative, it is a good example for studying the finite volume formulation, as will be described later.

## B. Initial Condition

The initial condition for the Burgers turbulence problem is defined by an initial energy spectrum in wavenumber space,  $E(k)$ , which is then converted to a velocity profile in wavenumber space,  $\hat{u}(k)$ . Finally, a fast Fourier transform (FFT) is used to convert the velocity to physical space,  $u(t)$ . The initial energy spectrum is given by:

$$E(k) = Ak^4 \exp(-(k/k_0)^2), \quad A = \frac{2k_0^{-5}}{3\sqrt{\pi}} \quad (2)$$

where  $k_0 = 10$  indicates the  $k$  coordinate at which the initial spectrum has its maximum. This definition ensures that the total kinetic energy  $\int E(k)dk = 1/2$  at the initial condition [1]. The velocity magnitude in wavenumber space is obtained from the energy spectrum by:

$$|\hat{u}(k)| = \sqrt{2E(k)} \quad (3)$$

To simulate turbulence, the velocity magnitude is multiplied by a random phase wave function:

$$\hat{u}(k) = \sqrt{2E(k)} \exp(i2\pi\psi(k)) \quad (4)$$

where  $\psi(k)$  is a uniform random number distribution between 0 and 1 that satisfies the conjugate relationship  $\psi(k) = -\psi(-k)$  [1]. This creates a unique initial turbulent condition. As shown in Figure 1, we will need to generate a number of solution samples that are averaged together to obtain a relatively smooth solution for the energy spectrum. Only having one sample, like the orange curve in Figure 1, produces a result that is difficult use for scheme comparisons.

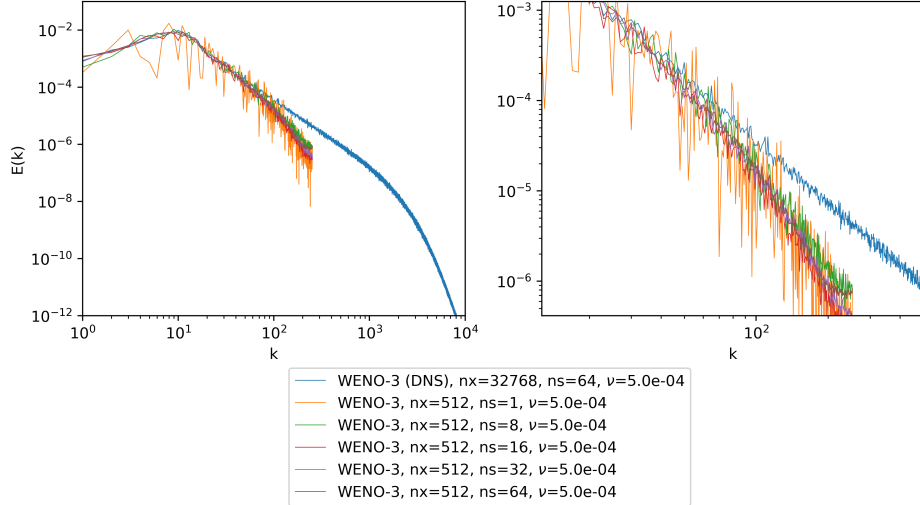


**Fig. 1 Comparison of number of samples, ns, used in 3<sup>rd</sup> order WENO results, t = 0s**

Once the initial velocity field is generated in wavenumber space, an FFT is used to convert to physical space,  $u(t)$ . This field can then be advanced in time using the subsequently defined numerical methods. In order to compare numerical schemes, we will obtain the kinetic energy spectrum in wavenumber space,  $E(k)$ , total kinetic energy,  $E(t)$ , and kinetic energy dissipation rate,  $-dE(t)/dt$ , defined by:

$$E(k) = \frac{1}{2}|\hat{u}(k)|^2, \quad E(t) = \int_{-k_m}^{k_m} E(k)dk, \quad -\frac{dE(t)}{dt} = \frac{E(t) - E(t - \Delta t)}{\Delta t} \quad (5)$$

## IV. Numerical Methods

### A. Finite Volume Formulation

As mentioned in section III.A, the finite volume formulation is well-suited for the Burgers turbulence problem. This is because it is flux conservative. To show this visually, Figure 2 shows nodes  $0 \leq i \leq NX$  at the centers of the finite volume cells. This is where quantities are stored. Fluxes cross the cell interfaces at nodes  $i \pm 1/2$ . The primary purpose of this study is to compare various schemes that reconstruct cell-centered quantities ( $i$ ) at the cell interfaces ( $i \pm 1/2$ ). As will be seen in the results, different schemes have different levels of dissipative effects on the solution. It should also be noted that it was chosen to use 2 ghost points on the lefthand-side of the domain ( $-2, -1$ ), and 3 ghost points on the righthand-side of the domain ( $NX + 1, NX + 2, NX + 3$ ). This definition becomes apparent in the wave speed definition in section IV.C.

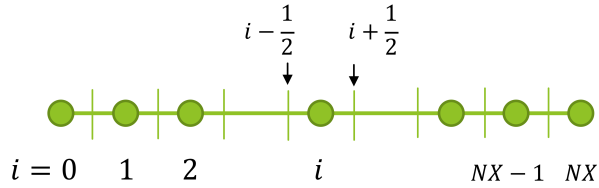


**Fig. 2 Finite Volume Formulation**

### B. Algorithm

To integrate and solve the viscous Burgers equation over time, we will use the following algorithm, which incorporates techniques like third-order Runge Kutta for time integration, a 4th order compact scheme for the second derivative, and various flux-based solvers for the inviscid term:

- Outer Loop, Time Integration (with index  $n$ ):
  - 1) Determine  $\Delta t$  for stability.
  - 2) Integrate over time to get  $u^n \rightarrow u^{n+1}$ :
    - Get viscous right-hand side (RHS) of update equation using 4<sup>th</sup> order compact scheme.
    - Get inviscid RHS using Rusanov Riemann solver and one of several finite volume reconstruction schemes.

We will first quickly go over the  $\Delta t$  determination, Runge-Kutta integration scheme, and 4<sup>th</sup> order compact scheme, before entering the focus of the paper: finite volume reconstruction schemes.

### C. Time Integration

To update  $u^n$  in time, we will use a 3<sup>rd</sup> order Runge Kutta algorithm, which is described by:

$$\begin{aligned} u^{(1)} &= u^n + \Delta t \cdot RHS(u^n) \\ u^{(2)} &= \frac{3}{4}u^n + \frac{1}{4}u^{(1)} + \frac{1}{4}\Delta t \cdot RHS(u^{(1)}) \\ u^n &= \frac{1}{3}u^n + \frac{2}{3}u^{(2)} + \frac{2}{3}\Delta t \cdot RHS(u^{(2)}) \end{aligned} \quad (6)$$

where  $RHS(u)$  is the right hand side of Eqn. 1 when rearranged for  $(\partial u / \partial t)$ . After each intermediate  $u^{(n)}$  calculation, periodic boundary conditions are enforced to ensure the ghost points on the left and righthand-sides of the domain are updated accordingly.

To integrate and obtain a stable solution, we must choose a  $\Delta t$  that meets the following stability criterion [1]:

$$\Delta t = CFL \frac{\Delta x}{\max(c_{i+1/2}^n)} \quad (7)$$

where  $c_{i+1/2}^n$  are the wave speeds at the cell interfaces,  $i + 1/2$ , given by:

$$c_{i+1/2}^n = \max (|u_{i-2}|, |u_{i-1}|, |u_i|, |u_{i+1}|, |u_{i+2}|, |u_{i+3}|); \quad 0 \leq i \leq NX \quad (8)$$

#### D. Compact Scheme for Second Derivative

To obtain the second derivative,  $u''$ , from the viscous portion of the governing equation, we will use the following 4<sup>th</sup> order compact scheme:

$$\frac{1}{10}u''_{i-1} + u''_i + \frac{1}{10}u''_{i+1} = \frac{6}{5h^2} (u_{i+1} - 2u_i + u_{i-1}) \quad (9)$$

which can be solved using a cyclic Thomas Algorithm [2].

#### E. Reconstruction Schemes for Solving Inviscid Burgers Equation

After using the compact scheme to solve for  $(\partial^2 u / \partial x^2)$ , we just need to solve for  $u(\partial u / \partial x)$  to complete the *RHS* for time integration. This can be found using the same techniques that would solve the inviscid Burgers equation:

$$\frac{\partial u}{\partial t} = -u \frac{\partial u}{\partial x} \quad (10)$$

There are two main methods to do this: reconstruction schemes (which we will be focusing on) and flux-splitting schemes. The idea is to reconstruct the cell-centered values,  $u_i$ , at the cell interfaces,  $u_{i+1/2}$ , using primarily nodes from either the left-hand or right-hand sides ( $u_{i+1/2}^L$  or  $u_{i+1/2}^R$  respectively). From there, we get the left and right fluxes,  $F^{L/R} = F(u_{i+1/2}^{L/R})$ , and solve for the flux at the cell interface using the Rusanov Riemann solver:

$$F_{i+1/2} = \frac{1}{2} (F^R + F^L) - \frac{c_{i+1/2}}{2} (q_{i+1/2}^R - q_{i+1/2}^L) \quad (11)$$

where here,  $q = u$ . Once we have  $F_{i+1/2}$ , the rest is simple:

$$u \frac{\partial u}{\partial x} = \frac{1}{\Delta x} (F_{i+1/2} - F_{i-1/2}) \quad (12)$$

The primary solution differences in this study are the different reconstruction schemes used to obtain  $u_{i+1/2}^{L/R}$ . While there are many not included here, we will focus on the MUSCL and WENO reconstruction schemes.

##### 1. MUSCL Reconstruction

One method for reconstructing quantities at the cell interface is called Monotone Upwind-Central Schemes for Conservation Laws (MUSCL). This method has many variants and makes use of flux limiters to prevent new maximums or minimums from arising in the simulation. A one-parameter MUSCL scheme can be described by [3]:

$$\begin{aligned} q_{i+1/2}^L &= q_i + \frac{1}{4} \left[ (1 - \kappa) \phi \left( \frac{1}{r} \right) (q_i - q_{i-1}) + (1 + \kappa) \phi(r) (q_{i+1} - q_i) \right] \\ q_{i+1/2}^R &= q_i - \frac{1}{4} \left[ (1 + \kappa) \phi \left( \frac{1}{r} \right) (q_i - q_{i-1}) + (1 - \kappa) \phi(r) (q_{i+1} - q_i) \right] \end{aligned} \quad (13)$$

where  $\kappa$  is a parameter that changes the type of MUSCL scheme,  $\phi$  is a limiter function, and

$$r = \frac{q_i - q_{i-1}}{q_{i+1} - q_i}$$

Because the parameter  $\kappa$  and limiter function  $\phi$  are able to be changed, a variety of MUSCL scheme variants can be formed using different values and combinations of values. The different types of MUSCL schemes studied in this paper are shown in Table 1, while the various limiter functions are described in Table 2.

**Table 1** Different types of MUSCL schemes formed by different choices of  $\kappa$  [3].

Scheme	$\kappa$ value(s)	Scheme	$\kappa$ value(s)
Quick:	0.5	KT:	1, -1
Central:	1	$3^{rd}$ Order:	1/3
Upwind:	-1	Fromm:	0

**Table 2** Different limiters and their definitions [3]

Limiter Type	Definition	
Van Leer	$\phi_{vl}(r) = \frac{r+ r }{1+r}$	$\lim_{r \rightarrow \infty} \phi_{vl}(r) = 2$
Van Albada	$\phi_{va}(r) = \frac{r^2+r}{r^2+1}$	$\lim_{r \rightarrow \infty} \phi_{va}(r) = 1$
Min-Mod	$\phi_{mm}(r) = \max(0, \min(r, 1))$	$\lim_{r \rightarrow \infty} \phi_{mm}(r) = 1$
Superbee	$\phi_{sb}(r) = \max(0, \min(2r, 1), \min(r, 2))$	$\lim_{r \rightarrow \infty} \phi_{sb}(r) = 2$
Monotonized Central	$\phi_{mc}(r) = \max(0, \min(2r, 0.5(1+r), 2))$	$\lim_{r \rightarrow \infty} \phi_{mc}(r) = 2$

## 2. WENO Reconstruction: $3^{rd}$ Order

Another method for reconstructing quantities at the cell interface is called the Weighted Essentially Non-Oscillatory (WENO) scheme. This makes use of smoothness indicators,  $\beta_k$ , which indicate the smoothness of the field on the left and right sides of node  $i$ . These are then used in conjunction with linear weights to construct nonlinear weights,  $w_k$ , which are used to determine which nodes will have the most impact on the reconstructed cell interface quantities. If there were a shock discontinuity on the left of node  $i$ , for example, the influence of those nodes would be weighted very small.

For the  $3^{rd}$  order WENO scheme, the smoothness indicators are defined by:

$$\beta_1 = (q_i - q_{i-1})^2; \quad \beta_2 = (q_{i+1} - q_i)^2 \quad (14)$$

The linear weights are defined by:

$$d_1^L = \frac{1}{3}, \quad d_2^L = \frac{2}{3}, \quad d_1^R = \frac{2}{3}, \quad d_2^R = \frac{1}{3} \quad (15)$$

The nonlinear weights are defined by:

$$\alpha_1 = \frac{d_1}{(\beta_1 + \epsilon)^2}, \quad \alpha_2 = \frac{d_2}{(\beta_2 + \epsilon)^2}, \quad w_1 = \frac{\alpha_1}{\alpha_1 + \alpha_2}, \quad w_2 = \frac{\alpha_2}{\alpha_1 + \alpha_2} \quad (16)$$

Finally, the  $3^{rd}$  order WENO reconstruction at the cell interfaces is given by:

$$\begin{aligned} q_{i+1/2}^L &= \frac{w_1}{2}(-q_{i-1} + 3q_i) + \frac{w_2}{2}(q_i + q_{i+1}) \\ q_{i-1/2}^R &= \frac{w_1}{2}(q_{i-1} + q_i) + \frac{w_2}{2}(3q_i - q_{i+1}) \end{aligned} \quad (17)$$

## 3. WENO Reconstruction: $5^{th}$ Order

For the  $5^{th}$  order WENO scheme, more nodes are required to reconstruct with increased accuracy. Whereas the  $3^{rd}$  order scheme requires nodes from  $i-1$  to  $i+1$ , the  $5^{th}$  order scheme requires nodes from  $i-2$  to  $i+2$ . Here, the smoothness indicators are defined by:

$$\begin{aligned} \beta_1 &= \frac{13}{12}(q_{i-2} - 2q_{i-1} + q_i)^2 + \frac{1}{4}(q_{i-2} - 4q_{i-1} + 3q_i)^2 \\ \beta_2 &= \frac{13}{12}(q_{i-1} - 2q_i + q_{i+1})^2 + \frac{1}{4}(q_{i-1} - q_{i+1})^2 \\ \beta_3 &= \frac{13}{12}(q_i - 2q_{i+1} + q_{i+2})^2 + \frac{1}{4}(3q_i - 4q_{i+1} + q_{i+2})^2 \end{aligned} \quad (18)$$

The linear weights are defined by:

$$d_1 = \frac{1}{10}, \quad d_2 = \frac{6}{10}, \quad d_3 = \frac{3}{10} \quad (19)$$

The nonlinear weights are defined by:

$$\alpha_k = \frac{d_k}{(\beta_k + \epsilon)^2}, \quad w_k = \frac{\alpha_k}{\sum_k \alpha_k} \quad (20)$$

Finally, the 5<sup>th</sup> order WENO reconstruction at the cell interfaces is given by:

$$\begin{aligned} q_{i+1/2}^L &= \frac{w_1}{6}(2q_{i-2} - 7q_{i-1} + 11q_i) + \frac{w_2}{6}(-q_{i-1} + 5q_i + 2q_{i+1}) + \frac{w_3}{6}(2q_i + 5q_{i+1} - q_{i+2}) \\ q_{i-1/2}^R &= \frac{w_1}{6}(2q_{i+2} - 7q_{i+1} + 11q_i) + \frac{w_2}{6}(-q_{i+1} + 5q_i + 2q_{i-1}) + \frac{w_3}{6}(2q_i + 5q_{i-1} - q_{i-2}) \end{aligned} \quad (21)$$

## V. Results

### A. MUSCL Variants & Limiters Comparison

When comparing different reconstruction schemes, it is useful to compare how much dissipation occurs after a certain period of time, in this case 0.05s. As shown in Figure 3, some schemes show higher levels of kinetic energy than others near the edge of the domain in wavenumber space. The more kinetic energy, the less dissipative the scheme is. For this study, a high resolution 3<sup>rd</sup> order WENO (WENO-3) solution was used as the "DNS" result to compare against. This is considered to be an accurate solution. Figure 3 shows all MUSCL-Central solutions with a limiter show some amount of dissipation, but the solution without a limiter actually has more kinetic energy than the DNS solution. This is because the absence of a limiter allows the numerical scheme to create new maximums and minimums, introducing error by *adding* kinetic energy. In this case, it is seen that the Monotonized Central limiter solution is closest to DNS, but in general, the Superbee limiter showed the best results (see Figure 4).

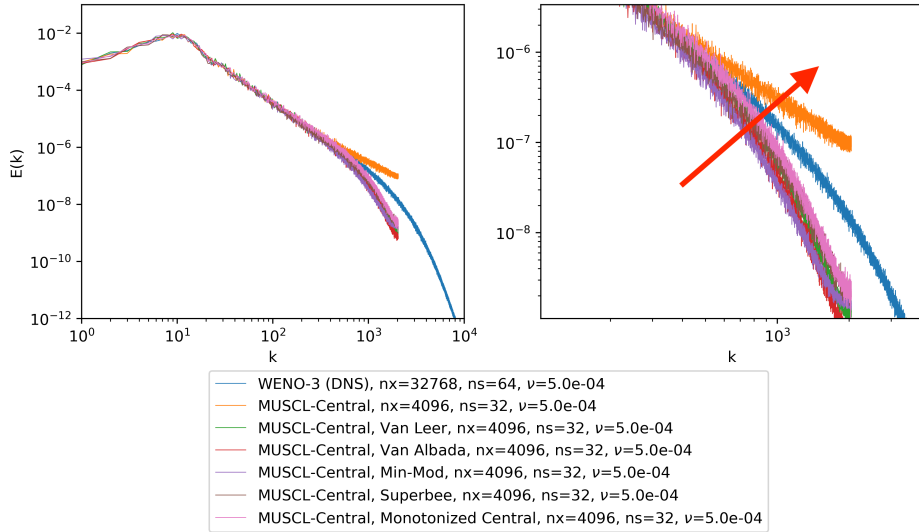


**Fig. 3 MUSCL-Central limiter comparison at  $t = 0.05s$ . The red arrow indicates that less dissipation occurs as solutions trend towards that direction. This is considered to be a desirable characteristic.**

Because Superbee showed the best performance of all the limiters, this was then used to compare all of the different MUSCL types. The results, shown in Figure 5, show that the type of MUSCL scheme has little impact on the results when this limiter is applied. More variation is shown between types, however, when no limiter is applied, as seen in Figure 6. Here it is shown that MUSCL-KT without a limiter correlates best with the DNS results. This will be used as the best MUSCL scheme to compare against WENO schemes in section V.C.

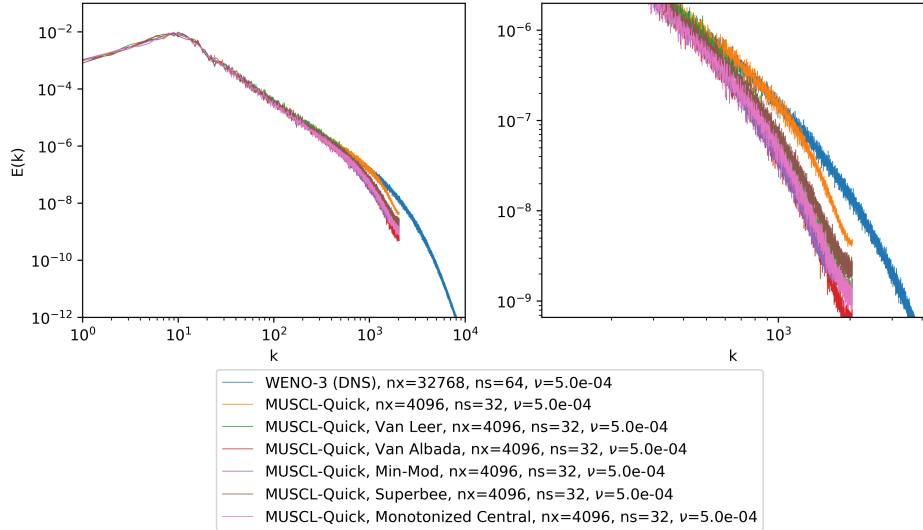


**Fig. 4 MUSCL-Quick limiters comparison at  $t = 0.05s$**

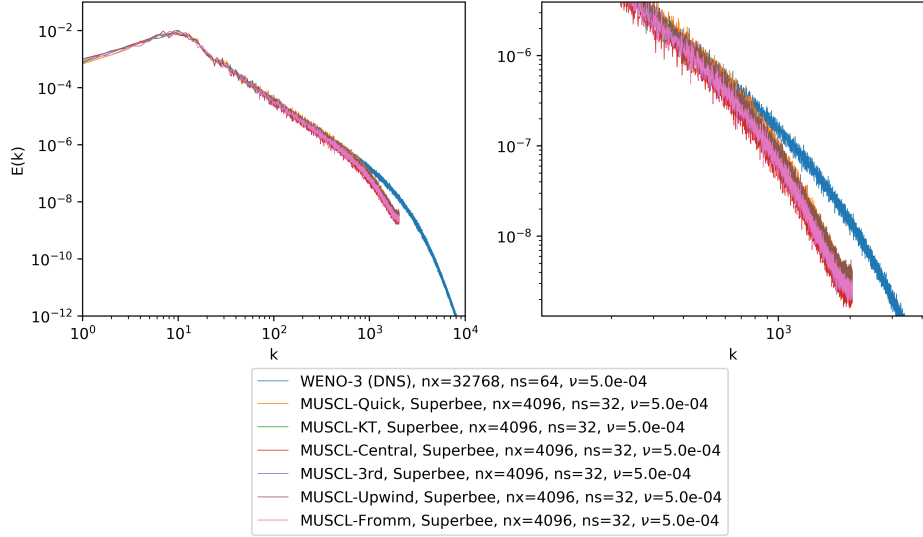


**Fig. 5 MUSCL type comparison with Superbee limiter,  $t = 0.05s$**

## B. WENO Resolution, Viscosity, and Order Comparisons

As discussed previously, the solution is considered less dissipative the closer it is to the DNS results. To show the effect that increasing resolution has on kinetic energy dissipation, Figure 7 was produced. This shows, as expected, that higher resolution solutions produce more accurate and less dissipative results. Additionally, it was investigated what effect viscosity had on dissipation, as seen in Figure 8. As expected, higher viscosity resulted in higher levels of dissipation.

The same type of analysis was carried out with the 5<sup>th</sup> order WENO scheme (WENO-5), and the results are shown in Figures 9 and 10 respectively. As can be see, all levels of resolution track fairly well with the WENO-3 DNS result except near the edge of the domain, where the solution shows dispersive characteristics. More information on this is discussed in section V.B.1. As shown by the viscosity comparison in Figure 10, more viscosity leads to more dissipation, as expected.

When comparing WENO-3 with WENO-5 at the same resolution, WENO-5 is shown to be much less dissipative than WENO-3, as seen in Figure 11. However,

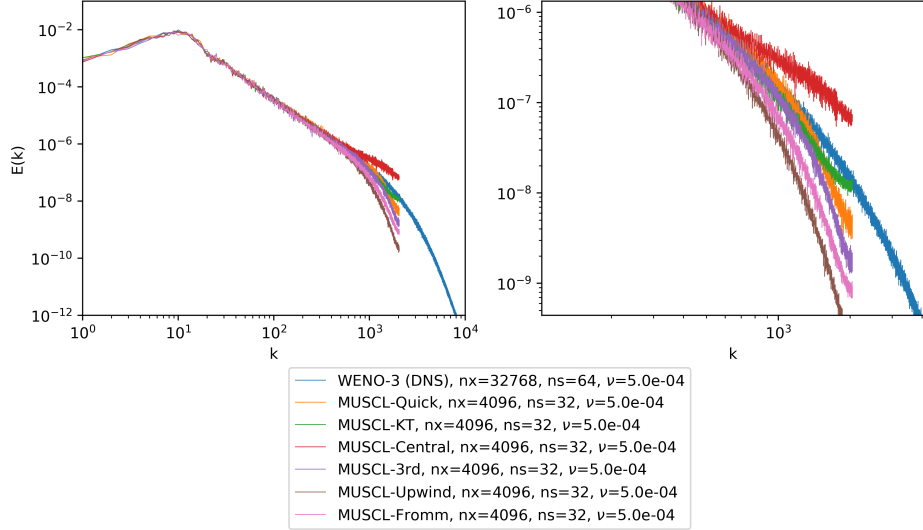


**Fig. 6 MUSCL type comparison without using a limiter,  $t = 0.05s$**

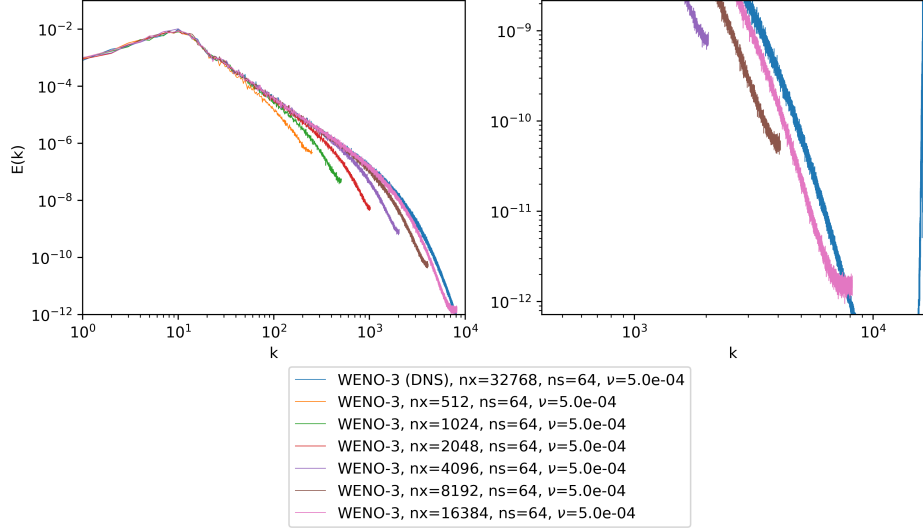


**Fig. 7 WENO-3 resolution comparison at  $t = 0.05s$**

### 1. WENO-3 vs. WENO-5 for DNS

With the decreased dissipation of the WENO-5 scheme, it might appear to be the better choice for to use as the DNS result to compare other schemes against. However, there are a couple of reasons it was not selected. First, the solution for total kinetic energy over time was generally smoother for WENO-3 than WENO-5 (see Figure 12a). Second, as shown in Figure 9, WENO-5 exhibits dispersion errors near the edge of the domain, making the solution less accurate at those points. This is also shown in Figure 12b, where WENO-5 is used as the "DNS" solution. The consistently dispersive behavior of WENO-5 was a key factor in choosing WENO-3 as the DNS solution.

### C. MUSCL vs. WENO Comparison

Finally, the best MUSCL scheme was compared against WENO-3 and WENO-5 at the same resolution and number of samples. The results, shown in Figure 13, show that WENO-5 follows the DNS result the closest. However, because of its dispersive characteristics outlined in section V.B.1, it would seem that MUSCL-KT can be considered the least dissipative scheme while remaining stable.

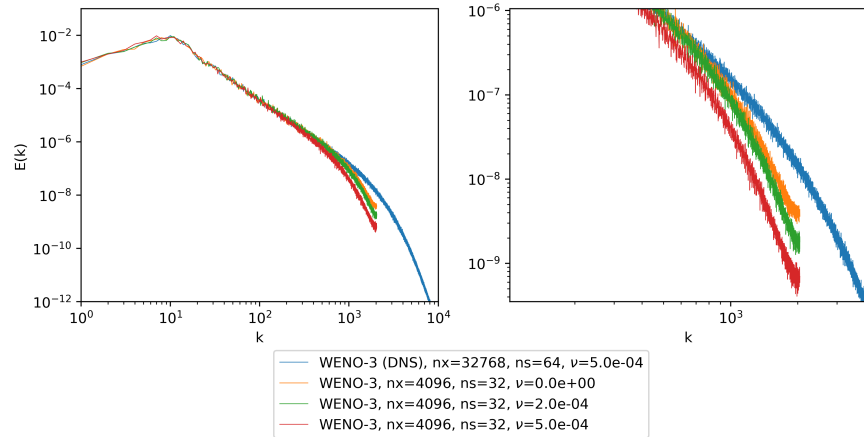


**Fig. 8 WENO-3 viscosity comparison at  $t = 0.05s$**

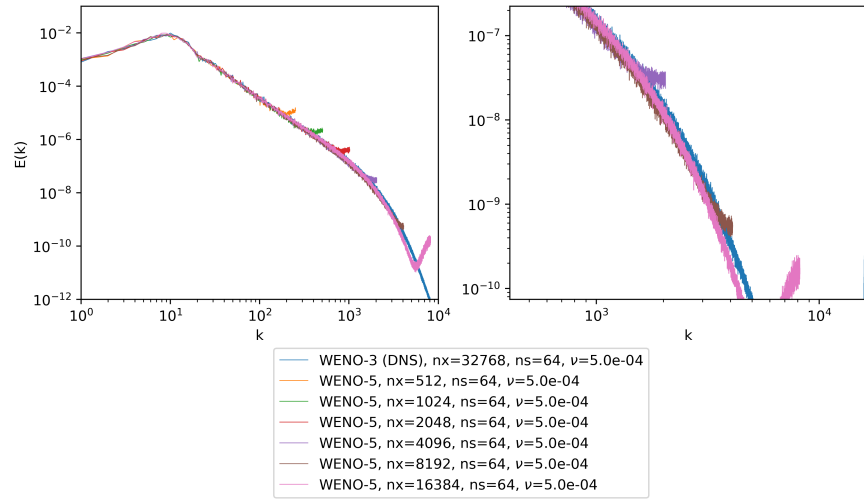


**Fig. 9 WENO-5 resolution comparison at  $t = 0.05s$**

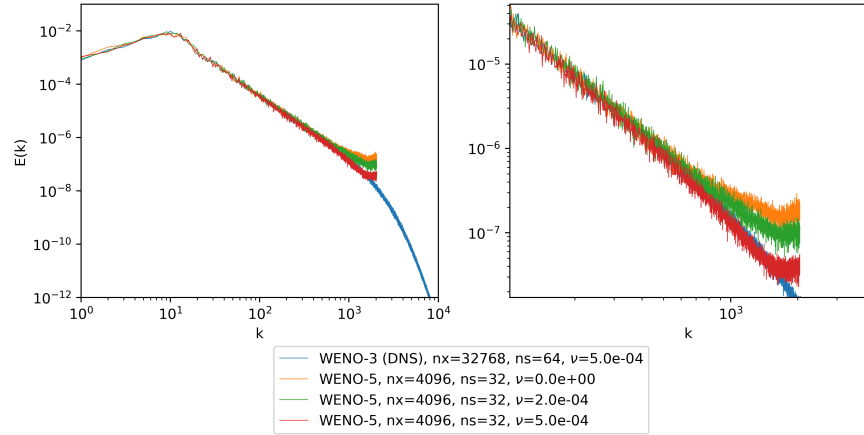


**Fig. 10 WENO-5 viscosity comparison at  $t = 0.05s$**

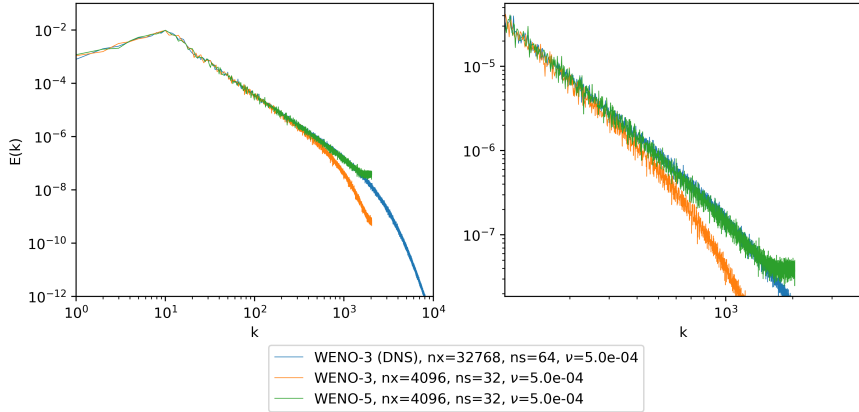


**Fig. 11 WENO order comparison at  $t = 0.05s$**

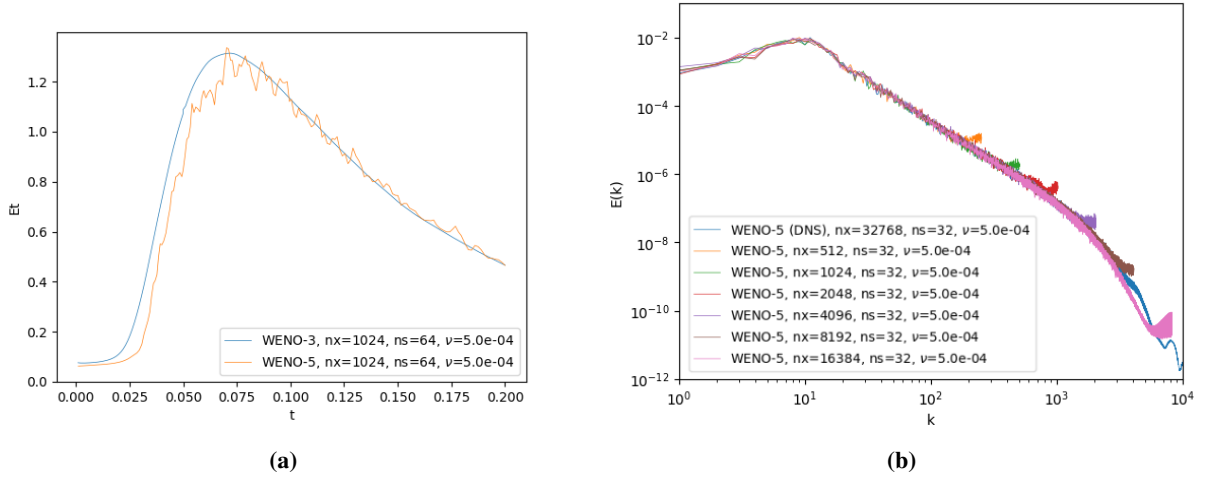


**Fig. 12 (a) WENO order comparison, kinetic energy dissipation rate at  $t = 0.05s$ ; (b) WENO-5 resolution comparison with WENO-5 as DNS solution,  $t = 0.05s$**

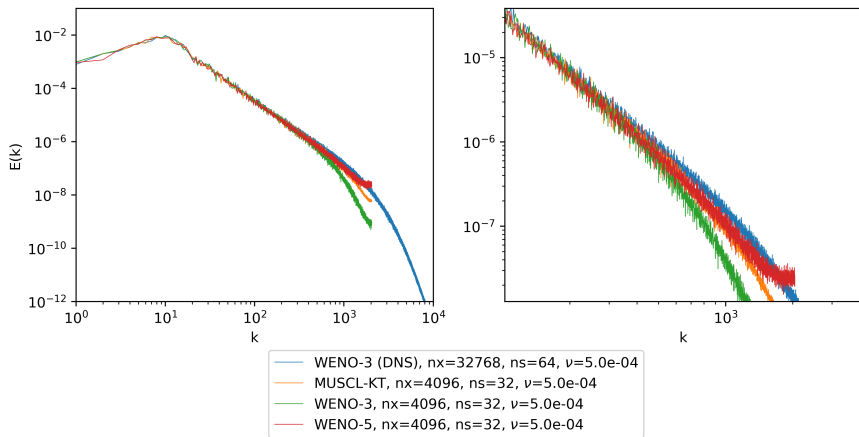


**Fig. 13 Best MUSCL scheme vs WENO-3 and WENO-5,  $t = 0.05s$**

## VI. Conclusions

In this study, various reconstruction schemes were investigated to compare their dissipative and dispersive characteristics when solving the 1D viscous Burgers turbulence problem. After analyzing many different MUSCL schemes, limiters, and WENO schemes, it was determined that the MUSCL-KT scheme with no limiter gave the least dissipative and dispersive solution for a given spatial resolution. Further studies could compare these against flux-splitting schemes and other reconstruction schemes. These could all be applied to a different set of initial conditions, such as a shock, to see how the different schemes perform for different scenarios.

## References

- [1] Maulik, R., and San, O., “Explicit and implicit LES closures for Burgers turbulence,” *Journal of Computational and Applied Mathematics*, Vol. 327, 2018, pp. 12–40.
- [2] Shanbhag, S., “Cyclic Tridiagonal Matrices,” , Mar 2014. URL <https://sachinashanbhag.blogspot.com/2014/03/cyclic-tridiagonal-matrices.html>.
- [3] San, O., and Kara, K., “Numerical assessments of high-order accurate shock capturing schemes: Kelvin–Helmholtz type vortical structures in high-resolutions,” *Computers & Fluids*, Vol. 89, 2014, pp. 254–276.